F61: Nuclear Magnetic Resonance

Paris J. Huth & Q'inich Figueroa

May 2024

Abstract

In the experiment we study properties and usages of nuclear magnetic resonance (NMR). Firstly we measure the characteristic relaxation times T_1 and T_2. This later was estimated with the Hahn echo and Carr-Purcell sequence. Both methods are compared. Secondly we used NMR to identify substances using with help of the characteristic chemical shift using TMS as reference substance. Lastly NRM was used for 1 dimensional and 2 dimensional imaging.

1 Theoretical and technical background

1.1 Basics of Nuclear Magnetic Resonance

Nuclear Magnetic Resonance techniques relay of the interaction between the magnetic dipole moment

$$\vec{\mu} = \hbar\gamma\vec{S} \tag{1}$$

of nuclei with non-zero spin S and an external magnetic field $\vec{B_0}$. In the following paper γ represents the gyro-magnetic ratio of protons:

$$\gamma_{proton} = 2.6752 \cdot 10^8 \,\mathrm{sec}^{-1}\mathrm{Tesla}^{-1}.$$

The resulting interaction energy, also called spin-lattice contribution, is defines as:

$$\Delta E = -\vec{\mu} \cdot \vec{B}_0. \tag{2}$$

This interaction yields two states for the orientation of the protons's magnetic dipole in the external magnetic field: μ_+ (parallel) and μ_- (antiparalle). For a macroscopic sample of N protons, both numbers of occupied states N_+ and N_-, the sum of which comprises N, can be approximated by a Boltzmann distribution , however $N_+ > N_-$, since the parallel state is energetically favorable. The predominance of protons in the parallel state leads to a macroscopic magnetization. In our case, a weak field ($\mu B \gg kT$), the ground state of the system can be approximated by

$$\vec{M}_0 = \frac{N}{V}\frac{\hbar^2\gamma^2 I(I+1)}{3kT}\vec{B}_0 \propto \frac{\vec{B}_0}{T}, \tag{3}$$

i.e the law of Curie.

In general, the magnetization can have an arbitrary orientation related to the external magnetic field, however such a system will decay asymptotically into the ground state, since $\vec{M}_0$ minimizes the energy.

The interaction between the macroscopic magnetization and the external magnetic field result in a torque

$$\vec{\tau} = \gamma \vec{M} \wedge \vec{B}_0. \tag{4}$$

If the magnetization is separated into parallel $\vec{M}_{\parallel}$ and perpendicular $\vec{M}_{\perp}$ components, relative to the external field, we quickly see that only the later gives a none trivial expression. Without any relaxation processes, the rate of change of the former is given by

$$\frac{d\vec{M}_{\perp}}{dt} = -\vec{M}_{\perp} \wedge \vec{B}_0. \tag{5}$$

The last equation describes the precession of $\vec{M}_{\perp}$ around $\vec{B}_0$. The angular frequency of this process is called Larmor frequency

$$\omega_L = \gamma B_0. \tag{6}$$

Generating a transverse or anti-parallel magnetization to $\vec{B}_0$ can be achieved by applying a high frequency pulse to the ground state magnetization $\vec{M}_0$. Let the static magnetic field $\vec{B}_0$ be pointing in z-direction. Now consider a coil oriented along the x-axis, if a sinusoidal voltage with frequency ω_H is applied it would generate a solenoid magnetic field $\vec{B}_1(t)$ polarized along the x-direction. Under this conditions the torque acquires a second term:

$$\vec{\tau} = \vec{M}_0 \wedge (\vec{B}_0 + \vec{B}_1(t) \tag{7}$$

which induces a second precession around the x-axis. For pulse duration which are short relative to the relaxation times, the magnitude of the magnetization is approximately constant. In this case the vector $\vec{M}$ moves in a sphere with radius $|\vec{M}_0|$. The vector coordinates in the sphere are then given by a azimuthal angle φ which is defined by the precession induced by $\vec{B}_0$, and by a polar angle θ which arise from interaction with the solenoid field. Both angles are a functions of time:

$$\varphi = \omega_L t \tag{8}$$

$$\theta = \gamma B_1 t. \tag{9}$$

A pulse which induces a polar angle $\theta = 90°$ is called a 90° pulse. For such a pulse the ground state magnetization is transformed into transverse magnetization $\vec{M}_{\perp}$. Analogously a pulse which generates $\theta = 180$ is called a 180° pulse. Such a pulse transforms the ground state into an anti-parallel magnetization $\vec{M}_{\perp} = -\vec{M}_0$.

1.2 NMR signal

1.2.1 Signal generation

In the set up used for this experiment the high frequency pulses of fixed frequency $\omega_{HF} = 19.8$ MHz were generated in a electronic unit of the minispec p20. Said pulses

induce a precession around de z-axis, as explain in the previous section, that change the magnetic flux through the coil in time resulting in a induction signal modulated by the Larmor frequency ω_L, which could be set up by hand. This signal is fed back to the p20 electronic unit, where both the high frequency and the induction signals are mixed into an output given by the multiplication of both inputs, i.g the sum of two cosine functions. One of the terms depends on the working frequency, which is given by the difference between ω_L and ω_{HF}, and is on the order of few hundred Hertz while the second one in the range of 40MHz. The use of a low frequency bandpass filter allows to get rid of the former signal.

1.3 Relaxation Time

1.3.1 Bloch equations

For the description of the precession of $\vec{M}_\perp$ it is possible to define a rotating reference system (x', y', z). This reference frame is defined by 2 condition: 1) the (x', y')-plane rotate in the static (x, y)-plane and 2) $\vec{M}_\perp$ points in the x'-direction.

In this reference system the transverse and longitudinal magnetization are constant if no relaxations processes are present, otherwise both components are time dependent. Their time evolution is described by the Bloch equations:

$$\frac{d\vec{M}_\perp^{rot}}{dt} = -\frac{\vec{M}_\perp^{rot}}{T_2} \tag{10}$$

$$\frac{d\vec{M}_\parallel^{rot}}{dt} = -\frac{\vec{M}_\parallel^{rot} - \vec{M}^{rot}}{T_1}. \tag{11}$$

The constant T_2 in eq. 10 is the so called spin-spin relaxation time whereas T_1 in eq. 11 is called the spin-lattice relaxation time. The ground state is equal in the rotating and the static reference frame.

In the presence of relaxation processed the time evolution of the magnetization in laboratory $\vec{M}$ and in rotating system $\vec{M}^{rot}$ are related giving the following Bloch equations in laboratory system:

$$\frac{d\vec{M}_\perp(t)}{dt} = \gamma(\vec{B} \wedge \vec{M})_\perp - \frac{\vec{M}_\perp(T)}{T_2}, \tag{12}$$

$$\frac{d\vec{M}_\parallel(t)}{dt} = \gamma(\vec{B} \wedge \vec{M})_\parallel - \frac{\vec{M}_\parallel(t) - \vec{M}_0}{T_1}. \tag{13}$$

1.3.2 Spin-spin relaxation T_2

Due to the magnetic interactions between the sample's protons with themselves, along with other phenomena, slowly varying field inhomogeneities are generated that cause the protons at different positions to precess with different frequencies. Hence a dephasing of the microscopic magnetization takes place, i.e $\vec{M}_\perp$ decays to zero. This process is called

spin-spin relaxation and it's characterized by T_2. Said decay is described by the solution of eq. 12:

$$\vec{M}_{\perp}(t) = \vec{M}_{\perp}^{0} e^{-\frac{t}{T_2}}. \tag{14}$$

In the following experiment two different methods were used to measure T_2: 1) spin-echo/ Hahn echo method and 2) Carr-Purcell sequence. In both cases a 180° pulse is used to reverse the dephasing.

Spin-Echo: The spin echo method consist on a 90° pulse that creates a transverse magnetization followed by a 180° pulse at $t = \tau$ that reverts the dephasing by exchanging the position of protons that presses faster with the slow ones. After the pulse all particles keep on rotating clockwise, such that at $t = 2\tau$ the fast protons catch up with the slow ones generating a spin-echo. The process is illustrated in Fig. 1. Due to Parseval's theorem

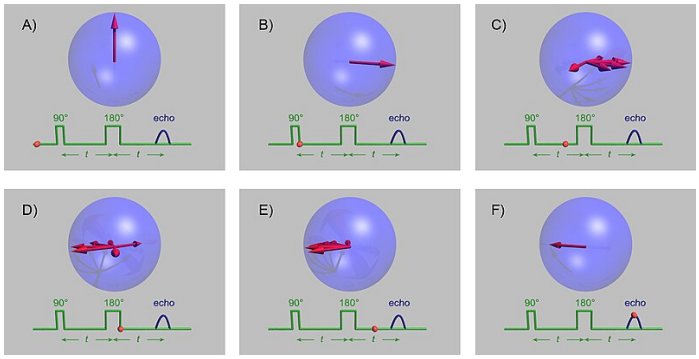

Figure 1: Spin-echo method. a) system in ground state, b) 90° pulse, c) dephasing, c) 180° pulse, d) rephasing, e) coherence/ spin-echo [1]

it is possible to estimate the signal's strength by calculating the are under the spin-echo curvature in frequency space. The decay curve of 12 is measured by varying the parameter τ in the 90°-180° sequence.

The Hahn echo finds its limitations when measuring the decay curvature for large t. In such cases the time evolution due to the field inhomogenieties is faster than the time scale of the measurement τ, i.g the average Larmor frequencies in time intervals $0 < t < \tau$ and $\tau < t < 2\tau$ can be different. Hence only partial coherence can be achieved leading to reduced signals and a reduced value for T_2.

Carr-Pulcell sequence: The Carr-Purcell methods consists of a 90° pulse that creates a transverse magnetization followed by repeated 180° pulse at odd multiples of τ that induce phase coherence at even multiples of τ as shown in Fig 2. In this case τ is a small time

[1] Nuclear magnetic resonance. (2024, May 16). Quelle: wikipedia.org

interval. The sequence is repeated over a large interval of time yielding a value closer to the real value of the spin-spin relaxation time in comparison to the spin-echo method.

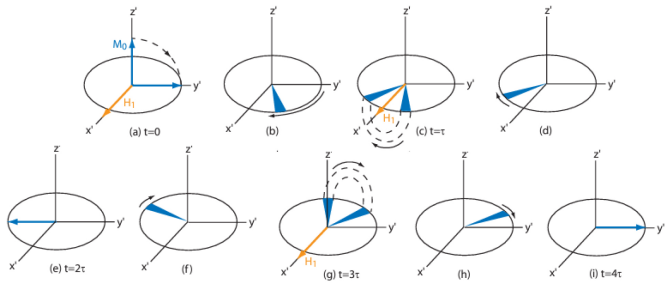

Figure 2: Carr-Purcell sequence. a) 90° pulse, b) dephasing of magnetization, c) 180° pulse at $t = \tau$, d) rephasing e) spin-echo/ coherence at $t = 2\tau$, f) dephasing, g) 180° pulse at $t = 3\tau$, h) rephasing, i) spin-echo at $t = 4\tau$. [2]

1.3.3 Spin-lattice relaxation T_1

An anti-parallel state will also decay by giving energy to its surroundings, this is the spin-lattice relaxation and it's described by the solution of 13

$$\vec{M}_{\parallel}(t) = \vec{M}_0 \left(1 - 2e^{t/T_1}\right). \tag{15}$$

After a 180° pulse a magnetization $\vec{M}_{\parallel}$ is generated, which is anti-parallel relative to the orientation of the field B_0. Since the an anti-parallel state doesn't produce a signal a 90° pulse at time $t = \tau$ is used to transform the magnetization into a transverse one. The signal at $t = \tau$ is proportional to the initial longitudinal state. The decay curve of $\vec{M}_{\parallel}$ can be measured by varying the value of τ in the pulse sequence 180°-90°.

1.4 Chemical shift

Protons that are bounded to molecules do not interact with the external magnetic field alone, but rather with a field $\vec{B}_{tot}$ modified by the magnetic shielding of the electron orbitals. Hence, according to equation 6, the Larmor frequency of the protons is also modified:

$$\omega_i = \omega_L \left(1 - \sigma_i\right). \tag{16}$$

Here ω_L is the free Larmor frequency, ω_i is the frequency modified by the chemical shift and σ_i stands for the shielding factor, which characterized the molecule and each nucleus within the molecule. In order to use this characteristic shielding factor to identify the

[2](2013, March 13). Physikalisches Praktikum im Bachelor-Studiengangander RWTH Aachen Versuch:Nuclear Magnetic Resonance(NMR) p. 16

molecule Tetra-Methyl-Silan (TMS) was used as reference substance. Under this condition the chemical shift δ_i is given by:

$$\delta_i = \sigma_i - \sigma_{TMS} = \frac{\omega_{TMS} - \omega_i}{\omega_L}. \tag{17}$$

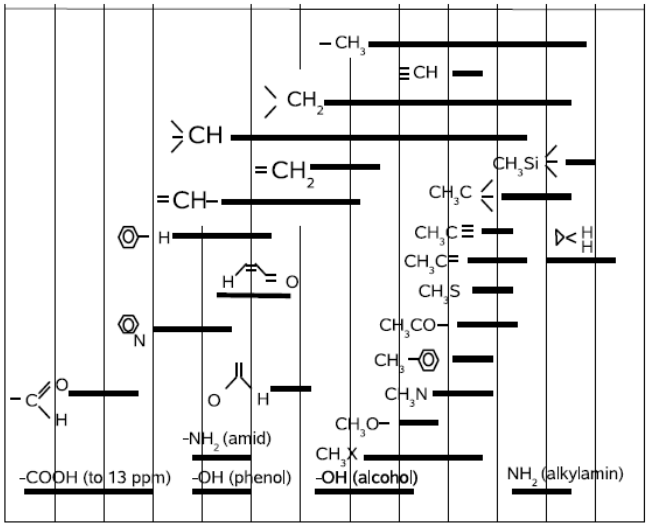

Figure 3: Chemical shift δ_i of differnt compounds relative to TMS [3]

s

1.5 Imagin with NMR

The imaging measurements in the experiment were made with the Bruker NMR analyzer mq7.5. In order to carry out measurements which contain information on the position of the produced NMR signal, position dependent fields are implemented. These fields are superimposed to the static field $\vec{B}_0$ which defines the z-axis. In the used set up all gradients are parallel to the static field and are linear functions of the corresponding coordinate.

$$\vec{B}^x = (0, 0, G^x \cdot x)^T$$

$$\vec{B}^y = (0, 0, G^y \cdot y)^T$$

$$\vec{B}^z = (0, 0, G^z \cdot z)^T$$

[3] R. Schicker (2021, March 4). Nuclear Magnetic Resonance F61/F62 p. 19

1.5.1 One dimensional imaging

Let's consider the 1 dimensional imaging in z-direction, where only the $\vec{B}^z$ is used.
Due to the field gradient the Larmor frequency becomes a linear function of position z:

$$\omega_L(z) = \gamma(B_0 + G^z \cdot z). \tag{18}$$

After taking the rotating frame into consideration, where $\vec{M}_\perp$ is given by 12 and will be denoted as $\vec{M}_\perp^{rot}$, and the position dependent Larmor frequency we can write the transverse magnetization as

$$\vec{M}_\perp(z,t) = M_\perp^{rot}(z,t)e^{i\gamma(B_0+G^z z)t}. \tag{19}$$

Using this expression one finds that the NMR signal is, apart from a phase factor, the Fourier transformation of the transverse magnetization $M_\perp^{rot}$:

$$S(t) \propto e^{i\Omega t}\int_V M_\perp^{rot}(z,t)e^{i\omega_z t}d\vec{x}. \tag{20}$$

Hence $M_\perp^{rot(z)}$ can be deduced from the measured NMR signal $S(t)$ by a 1 dimensional Fourier transformation signal.

For the measurements there exist two methods to generate the data points:

Frequency coding In this case the signal is measured a function on time and we sample over times $t_n = n\Delta t$ which give the data set:

$$S_1 = S(\Delta t), \quad S_2 = S(2\Delta t), ..., S_N = S(N\Delta t)$$

Phase coding In this approach we use the fact that during the readout the position information is related to the phase angle produced by the applied gradient:

$$\Delta\phi(z) = \phi(z) - \phi(0) = \gamma G^z z t = \omega_z t. \tag{21}$$

Thus the gradient G^z is applied during a time interval T_{Ph} before the read out, which induce a phase angle

$$\phi(z) = (\gamma G^z T_{Ph})z = k_z z. \tag{22}$$

Here k_z is the position frequency. After this time the gradient is switched off. All the components of the magnetization presses on with the original frequency but with different phase angles. To generated the data points the NMR signal is measured at a fixed time t_0 and sample over different position frequencies $k_n = n\Delta k$ by varying the gradient strength in steps ΔG^z. This results in the data set:

$$S_1 = S(\Delta k_z, t_0), \quad S_2 = S(2\Delta k_z, t_0), ..., S_N = S(N\Delta k_z, t_0).$$

1.5.2 Two dimensional imaging

For two dimensional imaging we use a two dimensional Fourier method. In this case the measurement method consist in first choosing a slice $z_1 < z < z_2$ which will be selectively excited by a high frequency pulse of duration t_p. At this point the different positions in the slice have different Larmor frequencies due to the slice selection gradient. To generate a phase coherent system a second high frequency pulse with opposite polarization and of duration $t_p/2$ is used. Consequently we implement a combination of phase coding in x-direction and frequency coding in y-direction to generate a matrix of NxM data points $S(k_n, t_m)$. Finally the image can be derived by a two dimensional Fourier transformation.

2 Measurements Procedure

2.1 Relaxation time

In this part of the experiment we study the relaxation times T_1 and T_2 of samples GD500 and GD600. For that we first start by calibrating the magnet of the p20 unit by inserting the GD600 sample and setting the 90° pulse for it to maximize the received signal. Analogously the 180° is set up for it to minimize the NMR signal. After calibration the measurements are taken as explain above: For T_2 we use the Hahn echo method and Carr-Purcell metod, whereas for T_1 we implement a 180°-90° sequence. During the entirety of this measurement the working frequency was set to $\omega_w = (1 \pm 0.5)$ kHz

2.2 Chemical shift

Next we use the NMR to identify 5 substances. For the identification of the probes we used TMS as a reference substance, hence we had two samples for each susbtance: one for the substance alone and a second sample mixed with TMS. The samples is inserted in the magnet of the p20 unit, then the probe was set in rotation with help of a air pump. This procedure was implemented to minimize the field inhomogeneities, hence minimazing the width of the signal in frequency space. Consequently we perform a spin-echo measurement. The signal is Fourier transformed and a Gauss profile is fitted into the different peaks of the spectrum to measure the frequency of the Maxima. These peaks correspond to the active groups of the molecule. The spectrum of the sample without TMS is compared to the one with TMS to identify the Maximum corresponding to the reference signal. Finally the relative distance between the TMS-maximum and the active group's maxima is measured. Using Fig. 3 we are able to identify the active groups. Once these are know we search for the matching molecules in Fig. 4.

[4]R. Schicker (2021, March 4). Nuclear Magnetic Resonance F61/F62 p. 20

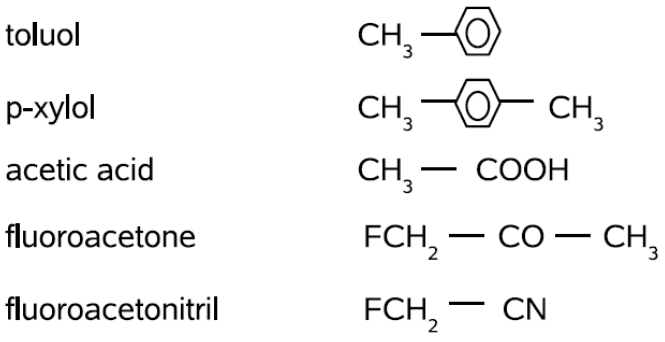

Figure 4: Five substances for identification [4]

2.3 Imaging

The last part of the experiment consist in 3 small tasks. All of them were performed using a Bruker minispec mq7.5 directly connected to computer.

1 dimensional imaging In this part we introduce three different samples and study their 1 dimensional profiles.

Time evolution of system We prepare a test tube with 15 ml of sand. About 4 ml of oil are poured in the test tube. The prepared vial is quickly placed into the NMRI device. To study the time evolution of this test tube we take different 1 dimensional profiles throughout a time interval.

2 dimensional imaging We place different objects in the NMRI machine and take 2D profile of them.

3 Results

3.1 Relaxation time

The variation of parameter τ in the spin-echo and 180°-90° sequence allowed us to measure the time evolution of the transverse, Fig. 5a & Fig. 5b, and anti-parallel magnetization, Fig. 7a & Fig. 7b. A second measurement for the transverse component using the Carr-Purcell sequence delivered Fig. 6a & Fig. 6b.

A quick glance at the curves already tell us that the time evolution of the components of the magnetization describe a decay curves, as we expected from the solutions of the bloch equations, eq.15 & eq. 14. By fitting these equation to our data we are able to find the characteristic relaxation times T_1 and T_2. See Tab. 1.

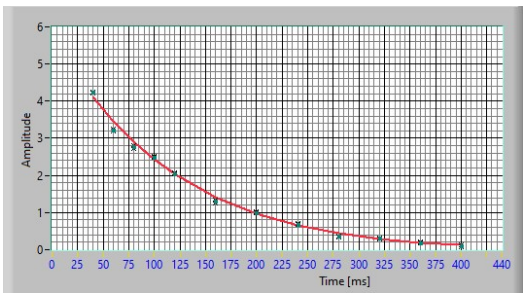

(a) GD500

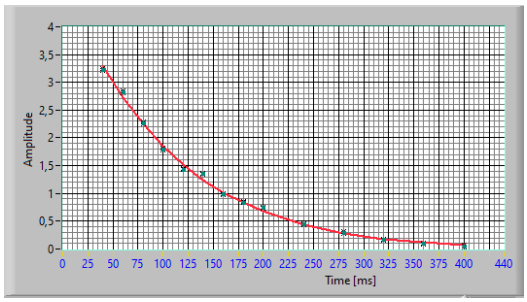

(b) GD600

Figure 5: Decay curve of $M_{\perp}$ measured with spin-echo methode

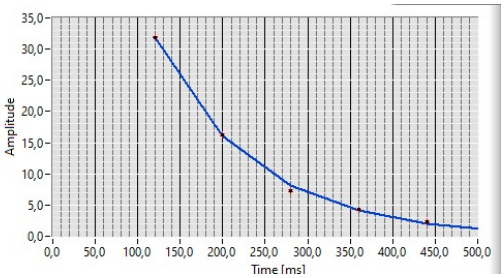

(a) GD500

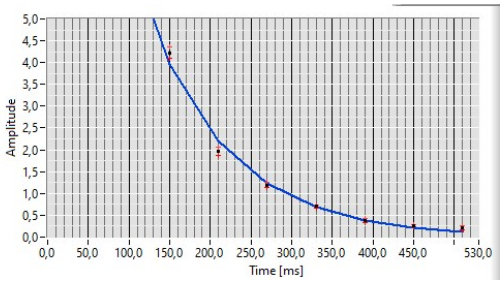

(b) GD600

Figure 6: Decay curve of $M_{\perp}$ measured with Carr-Purcell sequence

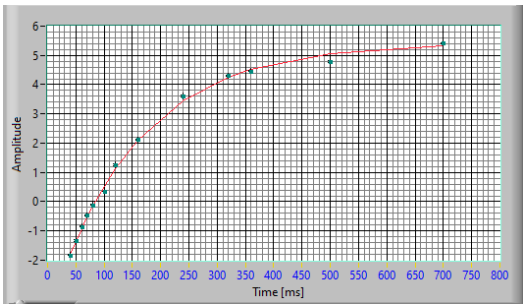

(a) GD500

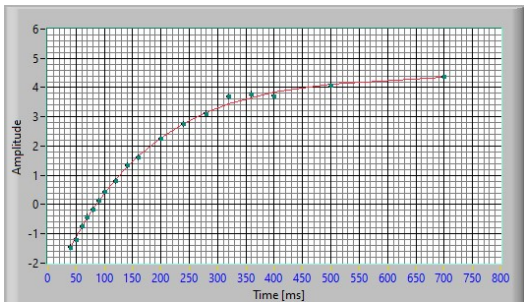

(b) GD600

Figure 7: Decay curve of $M_{\parallel}$ measured with 180°-90° sequence

Table 1: Relaxation times for Gd500 and Gd600

Probe	spin-spin T_2 [ms]			spin-lattice T_1[ms]
	spin-echo	Carr-Purcell	deviation σ	
Gd 500	110 ± 6	111,3 ± 1,5	0,5	159 ± 1,3
Gd 600	115,7 ± 1,2	116,9 ± 0,9	0,8	154,4 ± 1,2

Firstly we observe that the spin-spin relaxation time of the probe with higher density, GD600, is larger than that of GD500, which contradicts our expectations. From our theory we know that T_2 is mainly determined by the interaction between the proton's spins. Hence the bigger the concentration, which translates to a larger amount of protons therefore of spins, the more possibilities there exist for a proton to dissipate its excitation energy resulting in a smaller spin-spin relaxation time. Secondly we observe that $T_{1,Gd500}$ $T_{1,Gd600}$, as we expected. Analogously to the case of T_2, a higher concentration also translates in a smaller spin-lattice relaxation time, since the excited state has a larger lattice in which it can dissipates its energy.

From our experiment we can observe that the deviation between the results gained by the spin-echo and Carr-Purcell methods are not significant, however from our theory we know that this second method delivers more exact results. The Carr-Purcell sequence is also a faster measurement technique since it can be completely automatized, thus reducing the susceptibility to human errors. Lastly we also observe a higher precision from this second method, it delivers a smaller uncertainty in all measurements. This last point is better observed by the measurements of Gd500 where the uncertainty of the spin-echo method is almost 4 times bigger than the one delivered by the Carr-Purcell sequence.

3.2 Chemical shift

The measured frequency spectra for the samples with and without the reference substance are to be seen in Fig.8 - Fig. 12.

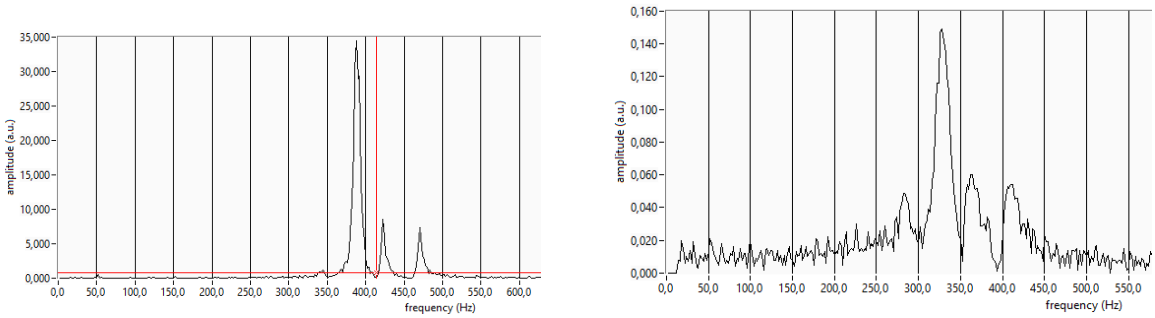

(a) Substance A

(b) Substance A + TMS

Figure 8: Frequency spectrum of substance A

The measured relative distances between the maximum of TMS and the active groups of the probes are in Tab. 2 along with then name of the molecule matching the found active groups. In the given list of molecules,see Fig. 4, we notice that fluroacetone is the only molecule with three maxima in its spectrum. Given its chemical components we expect one maximum corresponding to CH_3 and two lines from FH_2. This line splitting arise from the extra magnetic energy given to this component. Therefore to identify probe A there is no need to measure the relative distances Δ_i meticulously, instead a qualitative study of

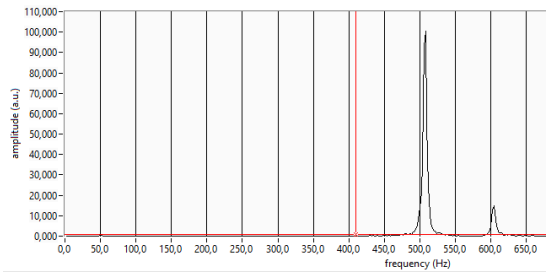

(a) Substance B

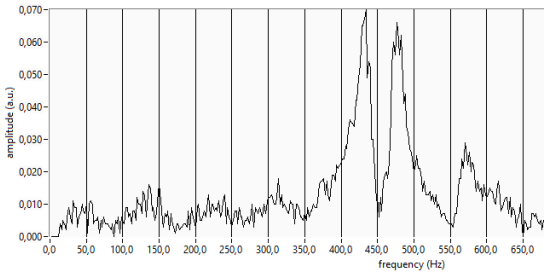

(b) Substance B + TMS

Figure 9: Frequency spectrum of substance B

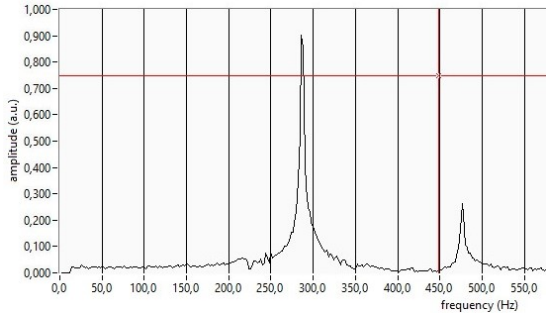

(a) Substance C

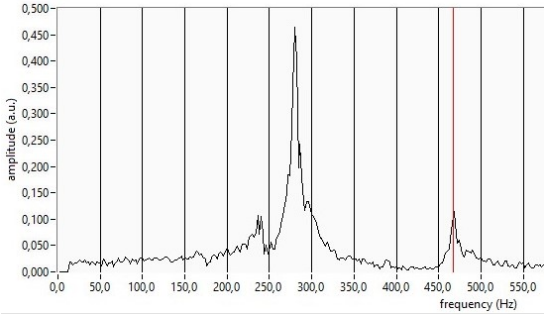

(b) Substance C + TMS

Figure 10: Frequency spectrum of substance C

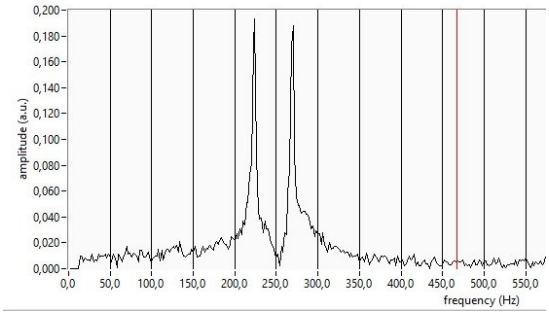

(a) Substance D

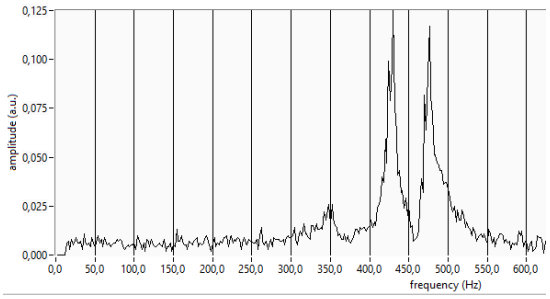

(b) Substance D + TMS

Figure 11: Frequency spectrum of substance D

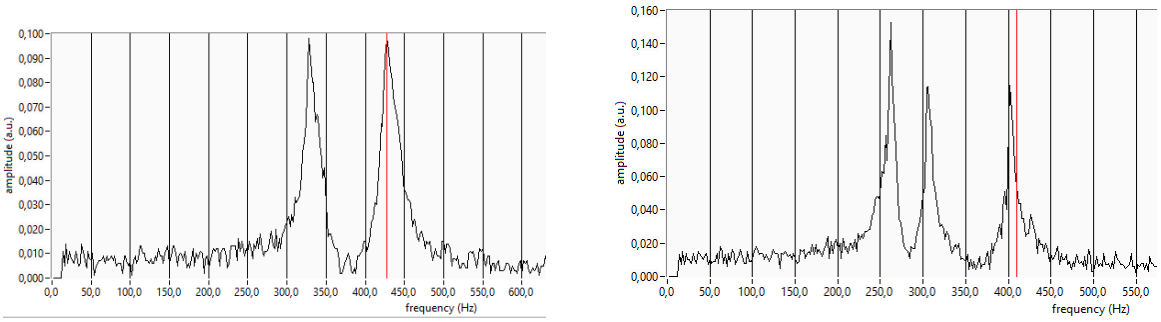

(a) Substance E (b) Substance E + TMS

Figure 12: Frequency spectrum of substance E

Table 2: Measured relative chemical and identification of probes

Probe	Relative distance Δ [ppm]			**Substance**
	Δ_1	Δ_2	Δ_3	
A	2,3	4,1	6,8	fluroacetone
B	2,5	7,2	-	p-xylol
C	2,2	11,8	-	acetic acid
D	4,1	6,5	-	fluroacetonitril
E	2,3	7,1	-	toluol

its spectrum, Fig. 8 is sufficient to identify it as fluroacetone. A study o f the measured relative chemical shift of D shows that it contains the 2 lines from FH_2 which leads us to identify it as fluroacetonitril. On the other hand, we can see in Tab. 2 that probes B and E have the same active groups, however we see a higher intensity in the peak corresponding to the active group CH_3 in the spectra of probe B, Fig. 9a, in comparison to that shown in E's spectra, Fig. 12a. With this observation we are able to identify substance B as p-xylol and E as toluol. Lastly we identify probe C as acetic acid due to the big chemical shift Δ_2, which is caused by the active group $COOH$

3.3 Imaging

1 dimensional imaging The signal obtained by a vertical imaging of two probe tubes containing the same oil show disparities, see Fig. 13. In the vial with less volume we see a constant signal, with some noise on top of it, meanwhile we observe a increase in the signal of the vial with higher volume of oil in range $x < -15$ mm and $x > 15$ mm. This sudden change in the measured signal is an effect caused by the non-linearity of the field gradient. It is know that the applied magnetic field is not perfectly linear. In conclusion, the probes have to be set in a position $x \in [-15 \text{ mm}, 15 \text{ mm}]$ in order to minimize the the effect of non-linearity of the field gradient.

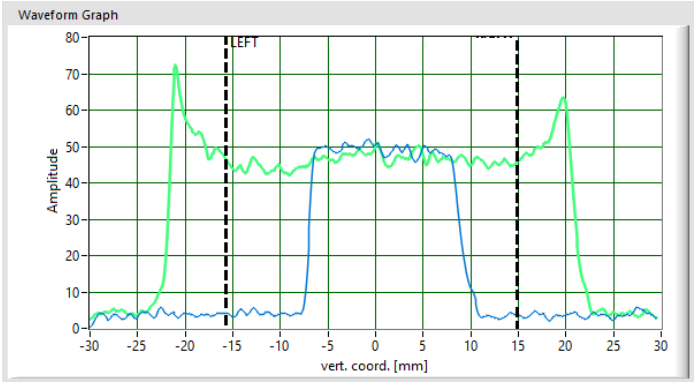

Figure 13: 1 dimensional NMRI of 2 oil samples. Blue line: short oil sample, green line: long oil sample

Secondly we insert a probe tube containing oil and a piece of teflon. The measured vertical profile, see Fig. 14, show a pattern of peaks and valleys which give us information about the structure of the teflon piece. Teflon does not emit an NMR signal, thus the pattern shown in the measured signal indicate that the used piece consists of stacked teflon plates. The valleys are generated by the presence of said plates. In this areas the signal is not zero since there still oil around the probe which does emit a NMR signal. In the other hand the peaks represent the areas where the plates are bonded to one another, and due to the higher volume of oil in such areas the measured signal is stronger.

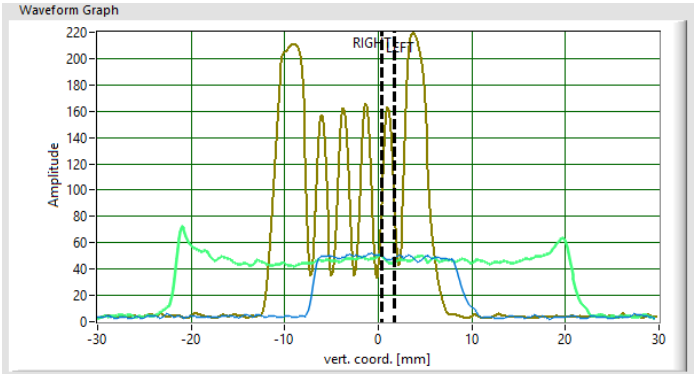

Figure 14: 1 dimensional NMRI of 2 oil samples & Teflon. Blue: short oil sample, green: long oil sample, brown: Teflon

Time evolution of system The vertical profile was measured in a time span of 96s. The NRM signal for times $t = 1, 10, 30, 50, 96$ are plotted in Fig. 15. In this diagram we observe how the position curve develops a concavity. We remember that the diffusion equation,

$$\frac{\partial u}{\partial t} = D\frac{\partial^2 u}{\partial x^2} \tag{23}$$

describes a convex curve. Therefore we conclude that the oil pouring down through the sand is not a diffusion process. Instead, the found time evolution is proper of a percolation process, which describes the movement and filtering of fluids through porous materials.

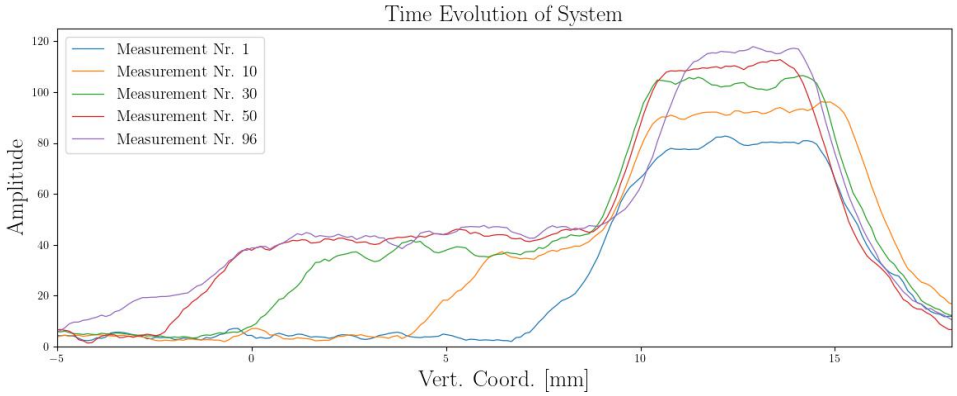

Figure 15: Time evolution of sand and oil probe.

2 dimensional imaging To get familiar with the measuring set up we started by taking horizontal and vertical scans of a vial filled with oil, see Fig. 16b & 16a. As expected, the

measured signals are constant at the position of the probe tube, thus the images show the geometry of the used probe tube.

When studying a peanut we first observe that due to the lack of water or fat in the nut's shell, it does not emit any NMR. Hence, in the taken scan we can only see the inner structures of the peanut. In the scans in Fig. 16c clearly observe both nuts and in the upper one we can descry the air gap between the two halfs of the nut. This gap can also be seen, with less resolution, in the horizontal scan, see Fig. 16d.

Analogously if we place a pecan in the NMRI device, the shell does not emit any NMR signal, thus we can only see the inner nut. See Fig. 16e.

Lastly we place a celery in the NMR machine, its horizontal profile can be seen in Fig. 16f. There we can see the C-shape of the branch. In the inner of the celery we also see slightly darker spots, which corresponds to holes filled with water. These spots are better visible in range $y \in [5, 20]$, however the resolution still not ideal.

4 Critical Discussion

The goal of the experiment is to study and get familiar with the theory and implementations of nuclear magnetic resonance. For that we studied two methods to measure the spin-spin relaxation time and one to estimate the spin-lattice relaxation time. Later we identify 5 probes by measuring the relative chemical shift, here we used TMS as reference substance. Next, we use NMR for imaging. In this last part we first get familiar with the machine by taking 1 dimensional scans, then we use 1 dimensional imaging to determine the nature of the time evolution of a system. Finally we use 2D imaging to map different objects and its structures.

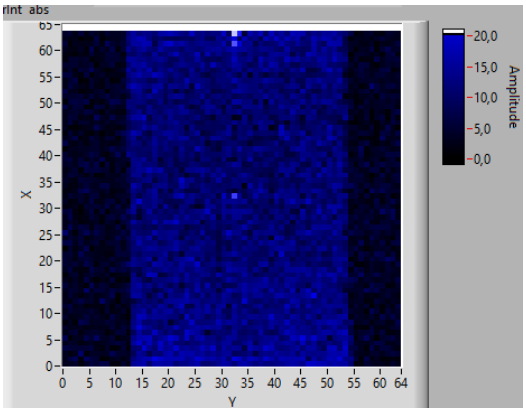

(a) vertical scan of oil

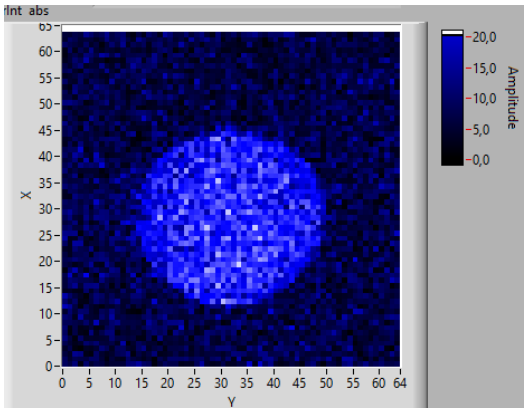

(b) horizontal scan of oil

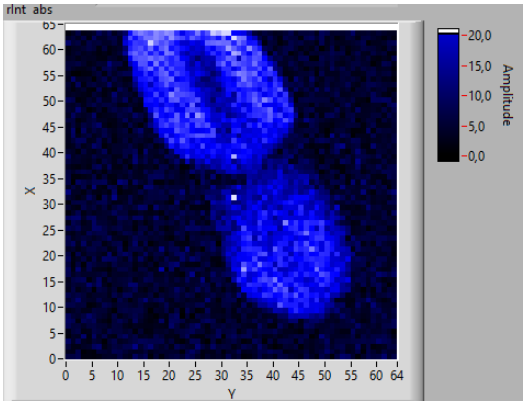

(c) vertical scan of peanut

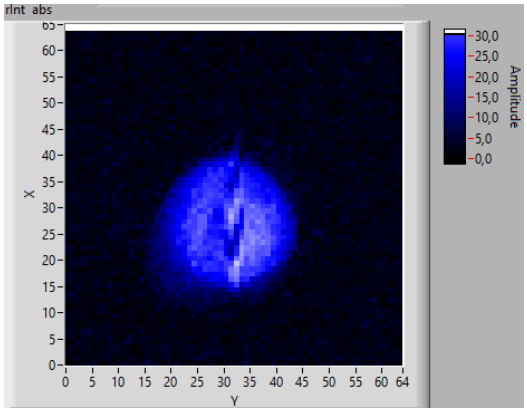

(d) horizontal scan of peanut

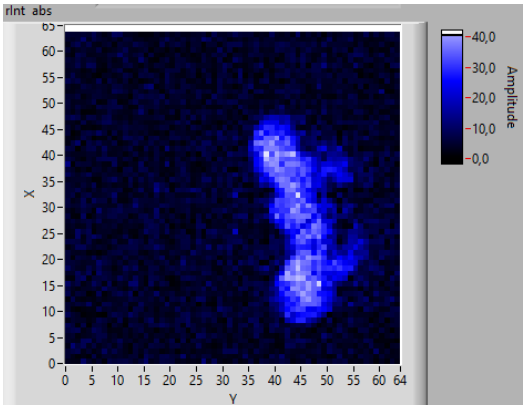

(e) horizontal scan of pecan

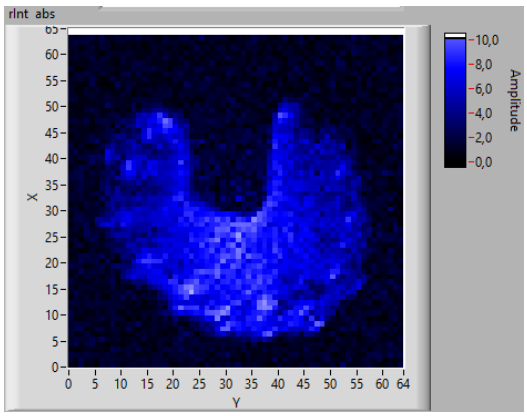

(f) horizontal scan of celery

Figure 16: 2D profiles of different objects